PNAS

Supporting Information for

Tracing Sources of Atmospheric Methane Using Clumped Isotopes

Authors: **Mojhgan Haghnegahdar, Jiayang Sun, Nicole Hultquist, Nora D. Hamovit, Nami Kitchen, John Eiler, Shuhei Ono, Stephanie A. Yarwood, Alan J. Kaufman, Russell R. Dickerson, Amaury Bouyon, Cedric Magen, and James Farquhar**

Corresponding author. Email: mojhganh@umd.edu

The PDF file includes:

Supporting text

Figures S1 to S19

Tables S1 to S9

References

Notation

The mass spectrometric measurement gives the following delta values normalized to the working reference gas using the following equations:

$$\delta^{13}CH_4 (\text{in } ‰) = 1000 \times \left(\frac{\left(\frac{^{13}CH_4}{^{12}CH_4} \right)_{sample}}{\left(\frac{^{13}CH_4}{^{12}CH_4} \right)_{reference}} - 1 \right), \quad (1)$$

$$\delta^{12}CH_3D (\text{in } ‰) = 1000 \times \left(\frac{\left(\frac{^{12}CH_3D}{^{12}CH_4} \right)_{sample}}{\left(\frac{^{12}CH_3D}{^{12}CH_4} \right)_{reference}} - 1 \right), \quad (2)$$

$$\delta^{13}CH_3D (\text{in } ‰) = 1000 \times \left(\frac{\left(\frac{^{13}CH_3D}{^{12}CH_4} \right)_{sample}}{\left(\frac{^{13}CH_3D}{^{12}CH_4} \right)_{reference}} - 1 \right), \text{ and} \quad (3)$$

$$\delta^{12}CH_2D_2 (\text{in } ‰) = 1000 \times \left(\frac{\left(\frac{^{12}CH_2D_2}{^{12}CH_4} \right)_{sample}}{\left(\frac{^{12}CH_2D_2}{^{12}CH_4} \right)_{reference}} - 1 \right). \quad (4)$$

We use the first two equations to represent $\delta^{13}C$ and δD. These are approximations because some ^{13}C and D are also in other isotopologues (like $^{13}CH_3D$, $^{12}CH_2D_2$) and are thus not accounted for. This introduces a shift much smaller than the analytical uncertainty relative to the actual definitions:

$$\delta^{13}C (\text{in } ‰) = 1000 \times \left(\frac{\left(\frac{^{13}C}{^{12}C} \right)_{sample}}{\left(\frac{^{13}C}{^{12}C} \right)_{reference}} - 1 \right) \text{ and} \quad (5)$$

$$\delta D (\text{in } ‰) = 1000 \times \left(\frac{\left(\frac{D}{H} \right)_{sample}}{\left(\frac{D}{H} \right)_{reference}} - 1 \right). \quad (6)$$

We also use:

$$\Delta^{13}CH_3D = 1000 \times \left(\frac{\left(1 + \frac{\delta^{13}CH_3D}{1000}\right)}{\left(\left(1 + \frac{\delta^{12}CH_3D}{1000}\right)\left(1 + \frac{\delta^{13}CH_4}{1000}\right)\right)} - 1 \right) \; and \quad (7)$$

, and

$$\Delta^{12}CH_2D_2 = 1000 \times \left(\frac{\left(1 + \frac{\delta^{12}CH_2D_2}{1000}\right)}{\left(\left(1 + \frac{\delta^{12}CH_3D}{1000}\right)^2\right)} - 1 \right), \quad (8)$$

to represent $\Delta^{13}CH_3D$ and $\Delta^{12}CH_2D_2$ respectively, and these also approximate to a high degree (much smaller than analytical uncertainty) the actual definitions:

$$\Delta^{13}CH_3D(in \text{ ‰}) = 1000 \times \left(\frac{\left(\frac{^{13}CH_3D}{^{12}CH_4}\right)_{sample}}{\left(\frac{^{13}CH_3D}{^{12}CH_4}\right)_{stochastic}} - 1 \right) \; and \quad (9)$$

$$\Delta^{12}CH_2D_2(in \text{ ‰}) = 1000 \times \left(\frac{\left(\frac{^{12}CH_2D_2}{^{12}CH_4}\right)_{sample}}{\left(\frac{^{12}CH_2D_2}{^{12}CH_4}\right)_{stochastic}} - 1 \right). \quad (10)$$

The approximations greatly simplify interconversion of Δ and isotopologue ratios that we use for the model calculations. In our exploration of the approximation, we have so far not found that the difference is expressed in the value well below the hundredths of a permil level.[*]

---

[*] We directly compared the two ways of calculating the values for combinations of $\delta^{13}C$, δD, and $\Delta^{12}CH_2D_2$ between 100‰ and -100‰ and $\Delta^{13}CH_3D$ between 5 ‰ and -5 ‰. We found that the difference between approximation and 'exact' was less than 0.00000001‰ for this range of values.

Sample types

Methane from air

Compressed air samples

Two samples of compressed air from a commercial air tank (Airgas) were analyzed (210419, 210421). The Airgas tanks are filled locally before sunrise, we were told by the facility. The facility is located at (38.92894 (^{o}N), -76.93319 (^{o}E)) which is next to a reconstructed wetland on the Anacostia river.

Urban air

Nine samples (210329, 210408, 21503, 21504, 210506, 211021, 210901, 210511, 210514) were collected in the UMD chemistry building by directly pumping from the makeup air duct. This air is actively blown into the makeup air ducts from an inlet outside the front door of the building (38.98938 (^{o}N), -76.94021 (^{o}E)). These samples were either connected directly to the preconcentration manifold or pumped into Tedlar bags that were then extracted. Most samples were extracted in the late morning after the nocturnal boundary layer had dispersed. One sample was collected into tedlar bags from the parking lot behind the College Park Shoppers Food warehouse (39.01690 (^{o}N), -76.92823 (^{o}E)) close to the freeway in the afternoon during a rush hour.

Air (local Mix) (enhanced methane levels due to local sources)

UMD Campus Farm location

Four samples were collected in the early morning by pumping air through tubes suspended from the silo at the UMD campus farm (38.99252 (^{o}N), -76.94038 (^{o}E)) at heights of 4 (210803-S4, 210720B, 210904s4) and 10 feet: (210803S10). At this time, the nocturnal surface boundary layer has not dispersed, which allows locally generated methane to accumulate. A fifth sample (210720S) was collected just across from the silo (38.99259 (^{o}N), -76.93983 (^{o}E)) in the afternoon. The samples were pumped into 200 L Tedlar bags. In these cases the samples were only 200 liters which leads to greater uncertainty on the measurements. In addition four samples were collected inside a three sided (open on one side) dairy barn (38.99252 (^{o}N), -76.94062 (^{o}E)) where cattle are kept

in pens (210803b3, 210803b2, 210801B1, 210423) in the morning. Due to limited air circulation and proximity to livestock and manure, these samples had higher proportions of local added methane. Note that a strong methane leak (from natural gas) was subsequently identified under the roadway by mobile surveys and the gas company. It is possible that this local leak could affect the samples, however the isotopologue data point to microbial sources. These samples were pumped into 200 L Tedlar bags using the Gast diaphragm pump.

Wetland sites

Two samples of air (210429, 210430/29) from a location on campus (38.99437 (^{o}N), -76.94431 (^{o}E)) by a regenerative stormwater conveyance and a third sample from a location at the Jackson Lane wetland (210418) (39.05744 (^{o}N), -75.75226 (^{o}E)) were collected by pumping air into 200 L Tedlar bags. The bags were returned to the lab and processed in the same way as other air samples. The samples collected on campus were collected at sunrise (before the nocturnal boundary layer had dissipated and convection up to cloud layers (planetary boundary layer) had been established). This allows for the locally sourced methane to accumulate to slightly higher concentration (a few hundred ppb above ambient). The sample from Jackson Lane was collected within a zone of flooded reed grass using off of a floating small platform in the late morning, which reduced mixing with ambient air. The Jackson Lane wetlands is an example of a type of seasonally-flooded freshwater wetland (a Delmarva Bays wetland) for which thousands are known across the Delmarva peninsula.

Other Methane Samples

Methane from Combustion

Two samples (210515a, 210515b/23) were collected from a covered grill by drawing smoke and air through a length of metal tube, attached to Tygon tubing using a Gast diaphragm pump and pushed into 10 L Tedlar bags. The bags were flushed twice with smoke before collecting the samples. For one sample, the grill was fed with oak logs and for the second sample, the grill was fed with charcoal.

Methane from chambers (wetlands and rice paddies)

Three samples (210420BC, 210420d/e, 210420H) were collected at the Jackson Lane Delmarva Bays wetland (39.05744 (^{o}N), -75.75226 (^{o}E)) and a fourth sample was collected in at the UMD campus (210409) (38.99437 (^{o}N), -76.94431) in two-piece chambers (14 inches wide, 24 inches long and 10 inches high when assembled that have an inlet and an outlet). The base of the chamber is pressed into the ground and left to sit before putting the top on. The top was put on and sealed. After a few hours, air was pulled from the chamber using a pump through the inlet with the outlet open (we used two pumps – a peristaltic pump and a Gast diaphragm pump. One sample (210819) was collected in an inverted funnel bubble sample from rice paddies east of Little Rock Arkansas, near 34.95659 (^{o}N), -91.30682 (^{o}E). For this sample, methane bubbles were collected in a 50 cc syringe.

Incubations

Three samples (210429i, 210430i, 210524i) were collected as incubations. The samples 210429i and 210430i were collected at the Jackson Lane wetland (39.05744 (^{o}N), -75.75226 (^{o}E)) and sample 210524i was collected at the campus regenerative stormwater conveyance location (38.99437 (^{o}N), -76.94431 (^{o}E)). For the first two incubation samples (210429i, 210430i) 100 cc of homogenized soil was loaded into autoclaved 200 cc serum bottles that were stoppered with blue silica stoppers. The serum bottles were successively evacuated, shaken, and filled with helium, and this was repeated three times. Once prepared the samples with helium headspace were placed in incubators at 32°C (210429i) or 25°C (210430i). The third incubation sample (210524i) was prepared by loading approximately 50 cc of mud with an additional 50 cc of water into an autoclaved 200 cc serum bottle sealed with blue silica stoppers. This sample was kept in 20°C. These three samples were left to incubate until sufficient methane accumulated in the headspace for analysis.

Natural Gas Samples

Three samples of natural gas were analyzed. Two of these were supplied by D. Rumble from the Marcellus (210516n) and Utica (212211n) shales and a third was collected from the wall of the lab (210506n) and was natural gas used for glassblowing. Because of their

high purity the first two of these samples were not processed through the purification line but were instead introduced directly into the Panorama. The third was purified and then analyzed.

Thermally-equilibrated samples

Three samples of gas were transferred by expanding at atmospheric pressure from a bag into sample tubes (with glass O-ring valves) containing 4-8 pellets of activated γ-alumina. Activation was done by heating the γ-alumina pellets in the tubes to >550°C. The tubes were then left for ~80 days at temperature to equilibrate. Temperatures of equilibration were 15°C, 32°C and 150°C. A fourth tube was set up at a temperature of 75°C, but the incubator containing the tube failed during the 80 days, cooling to room temperature.

Measured isotopic compositions of all samples are given in **Tables S1,S2, S3.**

Standardization of isotopic and isotopologue data

We standardized our isotopic data through analysis of calibrated samples from MIT (δ^{13}C and δD) and combined this with three thermal equilibration experiments undertaken using γ-alumina. Using this hybrid calculation, our measurements of the MIT reference gases are within error of most reported MIT values. The one exception is our measurement of Δ^{12}CH$_2$D$_2$ for AL1-CD which is outside of the 2σ overlap of the respective measurements. We do not have an explanation for this outlier. We found the thermal equilibration experiments to be challenging due to small shifts in the δ^{13}C and δD of our gases for experiments with γ-alumina and larger shifts for experiments we undertook with Pt wire and Ni metal. Our working hypothesis is that there are reactions between CH$_4$ with (or promoted by) the catalysts that we were unable to avoid, and this implies that further refinement in our calibrations may occur in our future work. See **Tables S2, S3, and S4** for isotopic data related to standardization and comparison with other labs.

Using Δ and δ notation to reveal evidence of mixing

Plotting clumped isotope data using delta notation provides information in a different way than the plots of Δ^{12}CH$_2$D$_2$ vs. Δ^{13}CH$_3$D (compare **Figure 1 and S1 with Figure S2**). On the δ ^{12}CH$_2$D$_2$ vs. δD plot the offsets for Δ^{12}CH$_2$D$_2$ are not obvious; however, the residuals (offset from the mixing line for air samples – which are straight lines on this plot) provide an illustration of

mixing and how some components do not fit. The principle is very similar to that seen for plots of $\delta^{13}C$ vs δD (e.g., main text **Figure 1**), but provides additional information about mixing endmembers and proportions. In this case, the compositions reflect mixing of methane from microbial sources into background tropospheric air.

Atmospheric Model

We used a box model to evaluate whether information from clumped isotopologues has the potential to provide information about changes in contributions from various (global-scale) sources. The model used simplified inputs for historical methane concentration data and for isotope compositions ($\delta^{13}C$ and δD). It assigns a single value for the sink by assuming a constant lifetime of 9.5 years. It also assigns smoothed (over time) values for various anthropogenic CH_4 fluxes (sources) that broadly follow those from two versions of EDGAR (1) and modifies the natural gas fluxes for these two using (2) to explore four different scenarios. The use of the same major isotope compositions and fluxes in all tests allows exploration of how changes in the proportion of fossil fuel methane (with positive $\Delta^{12}CH_2D_2$) to microbial methane (with negative $\Delta^{12}CH_2D_2$). The use of smoothed 5th order fits for most ($\delta^{13}C$ excepted -see below) inputs reduces expression of non-steady-state model response that generate short term shifts in $\Delta^{12}CH_2D_2$.

Concentration data used for atmospheric model:

We fit a 5th order polynomial to the annual global methane concentration data [reference data found at: https://gml.noaa.gov/webdata/ccgg/trends/ch4/ch4_annmean_gl.txt] that broadly follows the year resolution NOAA data record (3) from 1984 to 2019 and used this as the starting point for the model. See **Figure S3** for fit.

Total Source flux and flux of unsubstituted (major) isotopologue

We simplify the treatment of isotopic compositions and their relationship to mixing proportions by assuming that methane concentration and the concentration of $^{12}CH_4$ are identical. This is not the case, but (3) have shown that this assumption can be used to calculate relationships between isotopes with only a small shift relating isotopes and concentration of the elemental species (e.g., methane in this case).

We solved for the total flux of methane into the atmosphere (E) by solving the equation for a box model with a first-order sink[†] (e.g. controlled only by methane concentration and with a constant lifetime) in terms of the flux (E) into the box: the following equation:

$$E = \frac{k\left(n_t - n_{t-1}e^{-kt}\right)}{\left(1 - e^{-kt}\right)}, \tag{11}$$

where n_t is the amount in the box at time (t), n_{t-1} is the amount in the box at the prior time step (t-1), and k is the first order rate constant for the sink reactions . For the global atmosphere, to follow the evolution of concentration seen in Figure S3, the total flux into the atmosphere solved using this box model is given by **Figure S4**.

Component Source fluxes

Four models (scenarios) of anthropogenic source fluxes were used (**Figure S5**). Two models were run with source fluxes that are smoothed versions that broadly fit the flux of anthropogenic sources as outlined in the Emissions Database for Global Atmospheric Research (EDGAR), EDGAR 5.0 and 6.0 (1). Another two model runs were run with source fluxes that broadly fit EDGAR 5.0 and 6.0 but with substituting the natural gas fluxes of Höglund-Isaksson (2) (labeled as HI). **Figure S6.** Illustrates the different profiles of the natural gas fluxes of the E50 and E50HI and the E6 and E60HI.

The way that the model works, this also means that the part of the fluxes for natural (wetlands) will be different to make up a different amount of the total flux. The EDGAR component fluxes were divided into classes that were then assigned their own isotopic compositions (described later in this section). These yield the same profiles for E60 and E60HI and then also for the E50 and E50HI, but different between the E50 and E60 pairs (**Figure S7.)**. The classification strategy is described in **Table S5** and while it likely can be improved, provides a way to account for different contributions that can be used to evaluate the way the system broadly responds to changes in model scenarios. The principal assigned difference between the different

---

[†]The sink assumes that the combined reactions with •OH, Cl•, O(^{1}D), as well as oxidation in soils does not vary with time. Preliminary exploration of our model shows less sensitivity to changes in the strength of sinks than to changes in sources. This is an area that warrants future investigation with more complex atmospheric models.

scenarios is the natural gas flux. **Figure S6** illustrates the difference in the natural gas flux term between the four different scenarios.

Carbon and hydrogen isotopes

The atmospheric burden of $^{13}CH_4$ and $^{12}CH_3D$ are determined by considering records of $\delta^{13}C$ (**Figure S8A)** and δD (**Figure S8B.)** in combination with the atmospheric concentration of total methane (**Figure S3)**. The fluxes of $^{13}CH_4$ and $^{12}CH_3D$ are solved by adjusting the lifetime using information about kinetic isotope effects associated with the sink reactions. The carbon isotope profiles broadly matched that used by (5) and is not fit to a 5th order polynomial (smoothed) to illustrate how derived model results such as $\Delta^{13}CH_3D$ are affected by short term uncertainties in isotopic composition that arise the calculation of $\Delta^{13}CH_3D$ for sources, and its dependence on $\delta^{13}C$. The hydrogen isotope evolution of atmospheric methane was fit using the curve in **Figure S8B**. which broadly matched (6), but with an extension for the most recent decade showing no subsequent change. This evolution follows a smoothed curve from 1984 to 2006 and then a rise to 2010, and constant values thereafter. Like the evolution of $\delta^{13}C$, the assigned evolution of δD is approximate.

Derived $\delta^{13}C$ and δD of source methane

Solving for fluxes requires additional information about the kinetics of sink reactions for each isotopologue, which are used in combination with the constraints on sink for the major isotopologue ($^{12}CH_4$) to derive the k for each isotopologue. While this simplification would not be used in a more sophisticated model, it is valid and allows us to simplify the model. The rate data (KIE and ratios of rates relative to major isotopologue) used in our calculations are given in **Table S6.** These values assume the major contribution to the KIE is ●OH with a small contribution from Cl●. Small changes in these KIE (within the range of the difference from experimental determinations can have an effect on the model-derived ^{13}C-containing isotopologues because they have values near unity (see **Figure S17**), but the effects related to D- substitutions do not significantly affect the model results because these values differ from unity.

Constraints on kinetic isotope effects (KIE=k_{12CH4}/k_i, where k_i is the rate constant of the isotopologue of interest) of Haghnegahdar et al, (7) were used to constrain the rates of these sink reactions for $^{13}CH_4$ ($\delta^{13}C$) and $^{12}CH_3D$ (δD) as well as other isotopologues (described in sections

below). These electronic structure calculations are made with the Gaussian 09 software package (EM64L-G09RevD.01 (*21*)). The calculated values match experiments reasonably well for the best constrained values when high level Møller-Plesset theory (MP2 (*22*)) are coupled with large basis sets. Using these KIE with the model isotopic evolution yields an evolution of the CH_4 flux (total methane emissions, integrated or total source) with the $\delta^{13}C$ and δD of **Figure S9**. This isotopic composition reflects the ratio of fluxes for $^{13}CH_4$ and $^{12}CH_3D$ relative to $^{12}CH_4$. (e.g., $\delta^{13}C$ relates to $^{13}CH_4/^{12}CH_4$)

Isotopic compositions of Anthropogenic fluxes

The isotopic composition of the anthropogenic flux for the different model scenarios was calculated by considering the individual component contributions to the flux as listed in tables from EDGAR and then reassigned to a category with an assigned isotopic composition (**Table S5 - above**). The isotopic compositions for the categories (**Table S7**) were assigned based on values provided in (10) for the δD and $\delta^{13}C$ and (7) for clumped isotopologues, with the exception that microbial sources clumped isotopologues were all set to a single model determined value. Using these isotopic compositions, the isotopic compositional evolution of the anthropogenic sources is given in **Figure S10**.

Isotopes and isotopologues of natural (wetland) part of methane flux

Calculation of the individual isotopologue fluxes of the natural (wetland) part was done in the same way as for the total flux, but by considering adjustments to the anthropogenic component fluxes that scale with isotopic compositions of (10) and then by calculating the needed isotopologue fluxes from the natural (wetland) part to close the mass balance (difference) relating the total (integrated) flux for each isotopologue. These were then converted into isotopic compositions using standard definitions. The resulting isotopic compositions for the natural (wetland) source are given in **Figure S11** and yields a source with variable isotopic composition with time. While the clumped isotopologue composition of the natural (wetland) part of the flux is calculated as a constant value to allow each model scenario to end with the air isotopic composition matching the assigned valued (**Table S8**), the $\delta^{13}C$ and δD are allowed to vary with time (**Figure S11** shows the resulting variation). This is required by the treatment and could in principle be justified as possible if one considers that there could be changes in the types of wetlands or proportions of high latitude, mid latitude, and equatorial wetlands.

Isotopologues of methane in air

The remaining part of the model calculation is the clumped isotopologue composition of CH_4 fluxes (anthropogenic part, natural (wetland) part, and total) as well as the methane in air. These are given in **Figures S12, S13,** and text **Figure 3**. The model evolution in **Figure S13**, shows that different scenarios start at different $\Delta^{12}CH_2D_2$ and $\Delta^{13}CH_3D$, with those having a greater proportion of fossil fuel sources starting at higher values than those with a smaller proportion of fossil fuel sources. All model scenarios have a steep rise in $\Delta^{12}CH_2D_2$ and $\Delta^{13}CH_3D$ which is attributed to the weakening of CH_4 fluxes which allowed a greater expression of the KIE. The flattening seen in the second decade of this century likely reflects the waning growth of methane in the 1990's. The reason for the difference in phasing (delay) for the flattening of the CH_4 concentration profile (**Figure S3**) and the flattening of the clumped isotopologue profiles (**Figures S12 and S13**) reflects the longer lifetimes of the doubly-substituted isotopologues. The broad conclusion is that the different scenarios with different histories of emissions (fluxes) from fossil fuels, altered the proportion of fossil/microbial methane and can be detected by measuring clumped isotopologues. Such measurements should be possible either with archived samples or samples of air that are isolated from the atmosphere, such as in Arctic firn.

Further exploration of clumped isotopologues and their relationship to fossil and microbial methane

To explore the role of fossil fuels further, a second set of scenarios was examined that starts with an anthropogenic endmember with proportions broadly similar to those of the smoothed E60 scenario (Black dashed line in **Figure S14A.**) having a steady rise in the anthropogenic contributions from 1984 to 2018. Additional scenarios were set up to flatten this profile (colored lines in **Figure S14A.**), while maintaining the same total flux by shifting the natural (wetland) component (**Figure S11B.**) This second set of models was solved for the isotopic compositions in the same way as the previous model scenarios were solved and yields the $\Delta^{12}CH_2D_2$ for air and source in **Figure S15** and for δD in the total flux (single solution) and the natural(wetland) part of the flux in **Figure S16.**

While these models are very simple, they yield results that suggest the derived $\Delta^{12}CH_2D_2$ and the δD of the total sources will be more constant in scenarios that include a rising influence of microbial CH_4 sources. If constancy is a more parsimonious state, it would suggest that the

clumped isotopes and the δD support a rise in wetland fluxes as the explanation for the most recent rise in atmospheric methane concentration. This is analogous to the recent proposals (11-14) based on δ^{13}C (and δD). These test scenarios also show the potential of $\Delta^{12}CH_2D_2$ in distinguishing between different scenarios and the accompanying δ^{13}C and δD.

<u>Note on KIE and uncertainty</u>

The main results reported in this study are based on second-order Møller-Plesset theory (MP2 (22)) determined in Haghnegahdar et al., (7). The KIE used for the calculations play a role in the results of the models and determination of KIE at high enough precision to be used in the calculations experiments has proven to be challenging. For example, experimental determination of the KIE for the $^{12}CH_2D_2$ + •OH and $^{13}CH_3D$ + •OH sink reactions at 298 K are 1.81± 0.28 (15) and 1.34± 0.03 (16), respectively. The KIE of the $^{12}CH_2D_2$+Cl· (17-21) have been determined to be 1.60±0.03 for $^{13}CH_3D$+Cl· (22). Whitehill et al. (23) define a term $^{i,j}\gamma_{OH}$ ($^{i,j}k*k/(^{i}k*^{j}k) = {}^{i}KIE*^{j}KIE/^{i,j}KIE$) that can be used to relate the KIE uncertainties to uncertainty on $\Delta^{13}CH_3D$ and $\Delta^{12}CH_2D_2$. Using Monte Carlo techniques, uncertainties for experimental determinations of KIE propagate to ±150‰ and ±20‰ for $^{2,2}\gamma_{OH}$ and $^{13,2}\gamma_{OH}$ (representing $\Delta^{12}CH_2D_2$ and $\Delta^{13}CH_3D$, respectively).

Ab Initio techniques offer another way to determine KIE which may be more precise for term $^{i,j}\gamma_{OH}$ ($^{i,j}k*k/(^{i}k*^{j}k) = {}^{i}KIE*^{j}KIE/^{i,j}KIE$) (and $\Delta^{13}CH_3D$ and $\Delta^{12}CH_2D_2$) because of cancellation of effects due to frequencies for all isotopologues (and resulting partition functions) are related by a single electronic structure model. The uncertainty for the KIE derived using ab initio techniques are evaluated by comparing results of calculations done at second-order Møller-Plesset theory (MP2) (22) and couple cluster single and double excitation (CCSD) (24) level of theory, yielding a difference on the order of 10‰ and 3‰, for $^{2,2}\gamma_{OH}$ and $^{13,2}\gamma_{OH}$ (respectively $\Delta^{12}CH_2D_2$ and $\Delta^{13}CH_3D$). Tunnel corrections for the •OH reaction made in previous studies (e.g. 4) amount to a smaller difference than the difference between MP2 and CCSD. Work to refine the KIE will improve the quality of results that doubly-substituted isotopologue measurements will ultimately have the potential to provide.

We undertook one calculation where we arbitrarily varied the KIE for the $^{13}CH_4$ sink reaction from 1.005 to 1.010, which is within the range of the experimental and theoretical studies. The KIE determined from ab initio studies used here is 1.006. What we find (**Figure S17**) is that a small shift in the KIE for the $^{13}CH_4$ sink reaction has an ~12‰ effect on the δ^{13}C generated

by the model for the natural (wetland) part of the source flux. This suggests that further investigation into the KIE is warranted because it has the potential to significantly reduce uncertainty associated with models considering $\delta^{13}C$.

<u>Description of apparatus</u>

The manifolds that we used for preconcentration and purification are illustrated in **Figure S18**. These were built as prototypes for air separation and purification. The manifold for preconcentration is in panel A. It consists of: a part for drying the air and restricting flow (canister with silica gel); a part for capturing methane (set of 6 ½ inch OD traps filled with HayeSep DB and cooled to liquid nitrogen temperature; a second set of HayeSep DB traps (not used); a U-trap to reduce CO_2, immediately before a final 3/8 inch OD Trap filled with HayeSep DB that is liquid nitrogen cooled for transfer of methane and air and then warmed with a -116°C ethanol slush while pumping for 30 minutes to finish the preconcentration. The system has been checked for methane by flow by connecting a bag with a T to an Aeris^{TM} gas analyzer to ensure no loss of methane during the preconcentration steps. The biggest issue we have encountered is incomplete transfer of methane from the HayeSep DB traps due to incomplete warming. The HayeSep DB is recommended, however, because for some samples with a nitrogen balance (incubations) we found that we were not able to reproducibly determine the isotopic composition if the trapping on silica gel resulted in saturation with nitrogen (had a residual pressure). Our hypothesis is that the competition by nitrogen for locations that would normally trap methane led to incomplete trapping of methane and fractionation. This was increasingly more important for low concentration methane samples. This has been addressed by flushing with dry nitrogen (the large traps) on transfer to the second trap, and by heating the second trap to 250°C when transferring the sample to the sample tube (panel B illustrates configuration). Panel C illustrates the purification manifold, which is similar to the manifold used by (25)) with three modifications. The GC, not pictured, is equipped with a molecular Sieve column that allows separation of oxygen, nitrogen, and Kr, from methane (**Figure S19**), the collection silica gel trap can be actively pumped when carrier is flowing, and the collection silica gel U-trap can be pumped through the central silica gel trap because of the rough pump configuration. In addressing the issue of Kr, we first set up the GC with a composite Mol sieve 5A column followed by a HayeSep D column and found that for separation of Kr, we needed to cool the column well below what the GC was designed for. This was done by drawing air and vapors from above a standing liquid nitrogen reservoir. We then

switched to a longer molecular sieve 5A column because of its properties for separation. The HayeSep DB trap is better for trapping and separating methane from nitrogen than silica gel.

Tests of isotopic fractionation during processing

We conducted two recent tests of recovery of methane as follows. We injected 1 cc of methane (40 micromoles) into a 200 L Tedlar bag filled with dry nitrogen. The contents of the bag were then drawn through the same procedure used to process air samples. Results are in **Table S9**. The larger uncertainty results from the smaller sample size. This sample size is 500 L of air. Tests of recovery with the purification line show recovery is better than 99%.

SI References

1. M. Crippa, et al., High resolution temporal profiles in the Emissions Database for Global Atmospheric Research. Scientific data 7, 121 (2020).
2. L. Höglund-Isaksson, Bottom-up simulations of methane and ethane emissions from global oil and gas systems 1980 to 2012. Environmental Research Letters 12, 024007 (2017).
3. X. Lan, K. Thoning, E. Dlugokencky, Trends in globally-averaged CH_4, N_2O, and SF_6 determined from NOAA Global Monitoring Laboratory measurements (2023).
4. A. L. Sessions, J. M. Hayes, Calculation of hydrogen isotopic fractionations in biogeochemical systems. Geochimica et Cosmochimica Acta 69, 593–597 (2005).
5. A. J. Turner, C. Frankenberg, P. O. Wennberg, D. J. Jacob, Ambiguity in the causes for decadal trends in atmospheric methane and hydroxyl. Proceedings of the National Academy of Sciences 114, 5367–5372 (2017).
6. A. J. Rice, et al., Atmospheric methane isotopic record favors fossil sources flat in 1980s and 1990s with recent increase. Proceedings of the National Academy of Sciences 113, 10791–10796 (2016).
7. M. A. Haghnegahdar, E. A. Schauble, E. D. Young, A model for $^{12}CH_2D_2$ and $^{13}CH_3D$ as complementary tracers for the budget of atmospheric CH_4. *Global Biogeochemical Cycles* **31**, 1387–1407 (2017).
8. M. Frisch, et al., Fox. Gaussian 09 (Revision E. 01). Gaussian. Inc., Wallingford, CT (2009).
9. A. Møller, M. S. Plesset, Note on an approximation treatment for many-electron systems.Phys. Rev. 46, 618–622 (1934).
10. O. A. Sherwood, S. Schwietzke, V. A. Arling, G. Etiope, Global inventory of gas geochemistry data from fossil fuel, microbial and burning sources, version 2017. Earth System Science Data 9, 639–656 (2017).
11. X. Lan, et al., Improved constraints on global methane emissions and sinks using $\delta^{13}C$-CH_4. Global Biogeochemical Cycles 35, e2021GB007000 (2021).
12. R. Fujita, et al., Global and regional CH_4 emissions for 1995–2013 derived from atmospheric CH_4, $\delta^{13}C$-CH_4, and δD-CH_4 observations and a chemical transport model. Journal of Geophysical Research: Atmospheres 125, e2020JD032903 (2020).
13. S. Basu, et al., Estimating emissions of methane consistent with atmospheric measurements of methane and $\delta^{13}C$ of methane. Atmospheric Chemistry and Physics 22, 15351–15377 (2022).
14. A. Milkov, S. Schwietzke, G. Allen, O. Sherwood, G. Etiope, Using Global Isotopic Data to Constrain the Role of Shale Gas Production in Recent Increases in Atmospheric Methane, Nature Scientific Reports, 10 (2020).
15. T. Gierczak, R. K. Talukdar, S. C. Herndon, G. L. Vaghjiani, A. Ravishankara, Rate coefficients for the reactions of hydroxyl radicals with methane and deuterated methanes. The Journal of Physical Chemistry A 101, 3125–3134 (1997).
16. L. Joelsson, et al., Kinetic isotope effects of $^{12}CH_3D$+ OH and $^{13}CH_3D$+ OH from 278 to 313 K. Atmospheric Chemistry and Physics 16, 4439–4449 (2016).
17. K. L. Feilberg, D. W. T. Griffith, M. S. Johnson, C. J. Nielsen, The ^{13}C and D kinetic isotope effects in the reaction of CH4 with Cl. Int. J. Chem. Kinet. 37, 110–118 (2005).
18. F. Sauer, R. W. Portmann, A. R. Ravishankara, J. B. Burkholder, Temperature dependence of the Cl atom reaction with deuterated methanes. J. Phys. Chem. A. 119, 4396-4407 (2015)

19. G. D. Boone, et al., Rate constants for the reactions of chlorine atoms with deuterated methanes: Experiment and theory. J. Phys. Chem. A. 105, 1456–1464 (2001).
20. Y. Matsumi, et al., Reaction and Quenching of Cl (2 P j) Atoms in Collisions with Methane and Deuterated Methanes. J. Phys. Chem. A. 101, 1216–1221 (1997).
21. T. J. Wallington, M. D. Hurley, A kinetic study of the reaction of chlorine atoms with CF_3CHCl_2, CF_3CH_2F, $CFCl_2CH_3$, CF_2ClCH_3, CHF_2CH_3, CH_3D, CH_2D_2, CHD_3, CD_4, and CD_3Cl at 295 K +/- 2 K. Chem. Phys. Lett. 189, 437–442 (1992).
22. L. Joelsson, et al., Relative rate study of the kinetic isotope effect in the $^{13}CH_3D+$ Cl reaction. Chemical Physics Letters 605, 152–157 (2014).
23. A. R. Whitehill, et al., Clumped isotope effects during OH and Cl oxidation of methane. Geochimica et Cosmochimica Acta 196, 307–325 (2017).
24. G. D. Purvis III, R. J. Bartlett, A full coupled-cluster singles and doubles model: The inclusion of disconnected triples. The Journal of Chemical Physics 76, 1910–1918 (1982).
25. E. D. Young, D. Rumble III, P. Freedman, M. Mills, A large-radius high-mass-resolution multiple-collector isotope ratio mass spectrometer for analysis of rare isotopologues of O_2, N_2, CH_4 and other gases. International Journal of Mass Spectrometry 401, 1–10 (2016).
26. E. D. Young, *et al.*, The relative abundances of resolved l2CH2D2 and 13CH3D and mechanisms controlling isotopic bond ordering in abiotic and biotic methane gases. *Geochimica et Cosmochimica Acta* **203**, 235–264 (2017).
27. Y. Gonzalez, et al., Precise measurements of $^{12}CH_2D_2$ by tunable infrared laser direct absorption spectroscopy. Analytical Chemistry 91, 14967–14974 (2019).
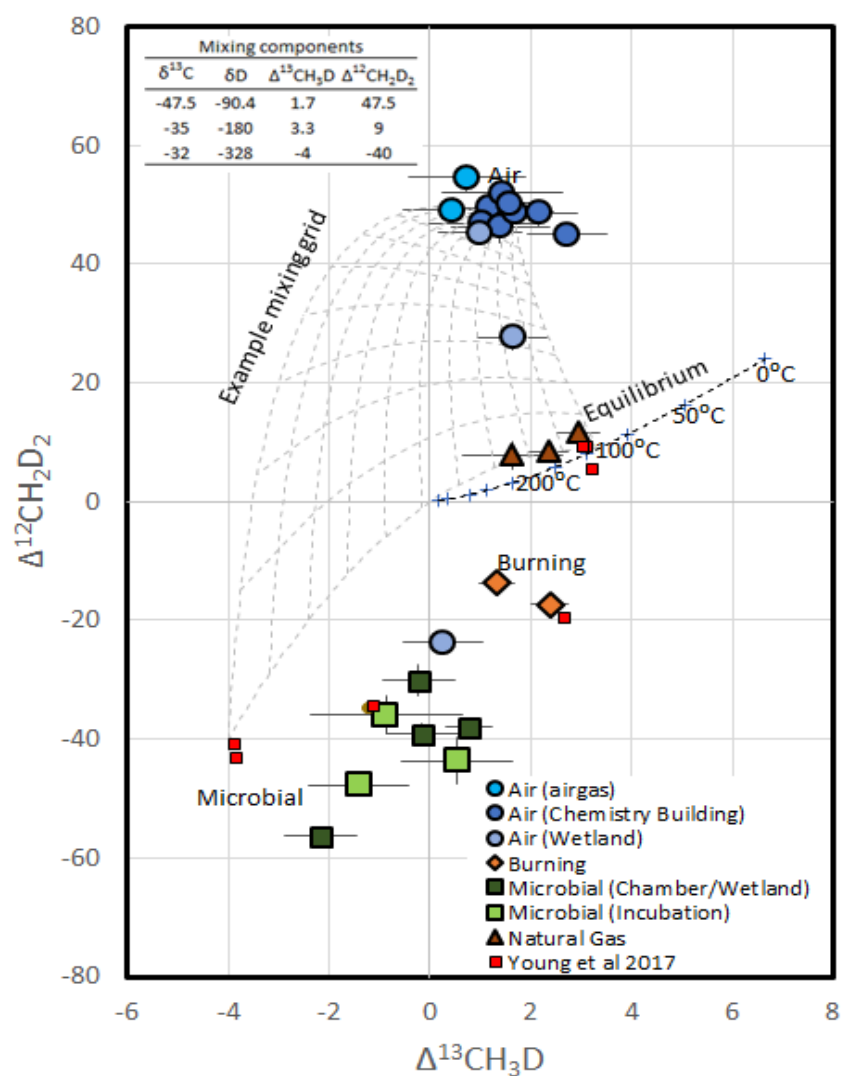
Fig. S1. Plot of $\Delta^{12}CH_2D_2$ vs. $\Delta^{13}CH_3D$ of methane samples measured in this study with a mixing grid added for mixing air with microbial and natural gas, both from (26). Also plotted on this figure in red are analyses from (26) for microbial cultures and natural gas samples. The air samples labeled wetland with low $\Delta^{12}CH_2D_2$ can be used for source composition identification and apportionment.
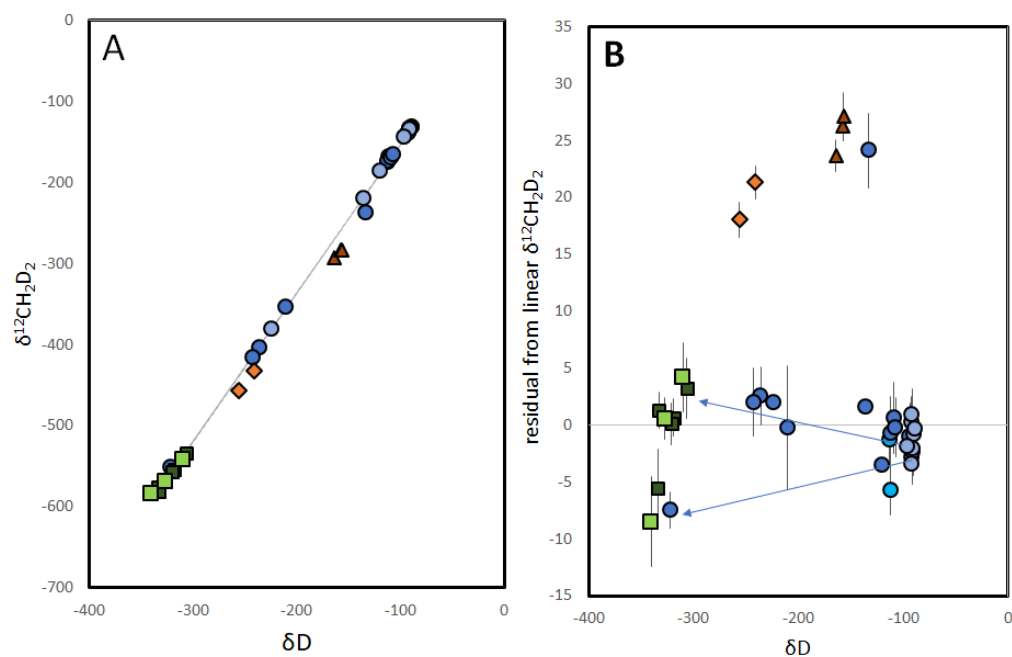
Fig. S2. A. Plot of $\delta\,^{12}CH_2D_2$ vs. $\delta\,D$ with mixing line fit for air samples. Note that data for natural gas and (biomass) burning lie away from this line. (Mixing is linear when isotopologues are plotted as delta values versus delta values.) **B**. Plot of the residuals relative to the mixing line to show that the different types of air mixing plot along different arrays. Symbols as in **Figure S1**.
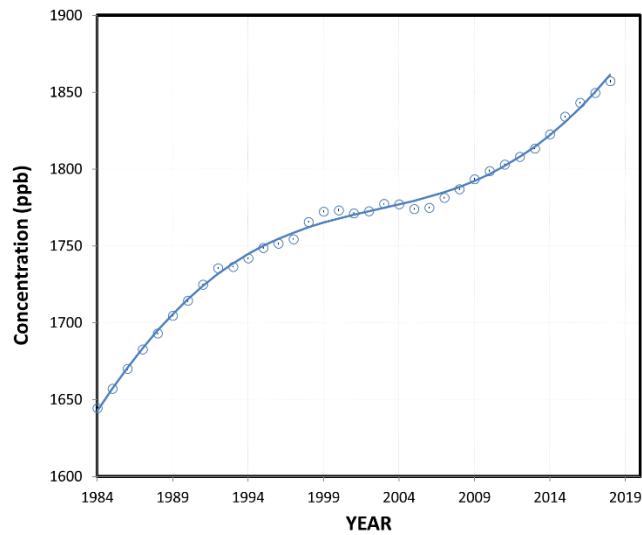
Fig. S3. Plot of methane concentration vs. time used for the model (5th order polynomial fit to data from https://gml.noaa.gov/webdata/ccgg/trends/ch4/ch4_annmean_gl.txt). Model is a line, data is presented as circles. Size of circles is approximately 3σ of the uncertainty on the data.
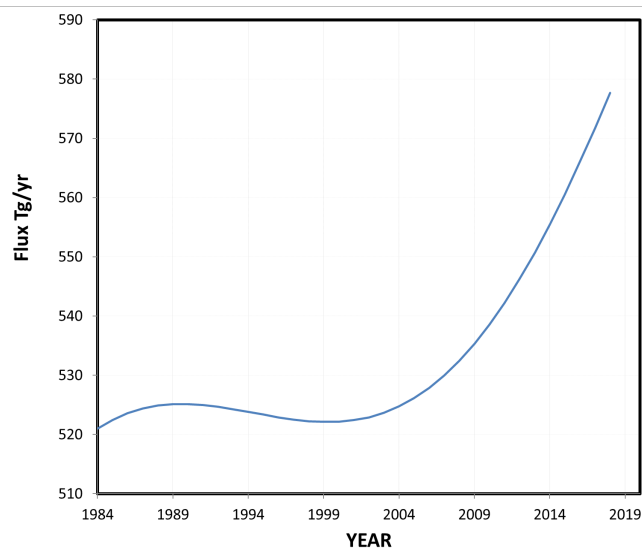

Fig. S4. Global CH_4 flux calculated using equation (11) from the concentration profile in **Figure S3.** These fluxes are assumed as the total for the major methane isotopologue ($^{12}CH_4$). While this is not strictly valid as the solution for the major methane isotopologue, it introduces only a small systematic uncertainty.

20
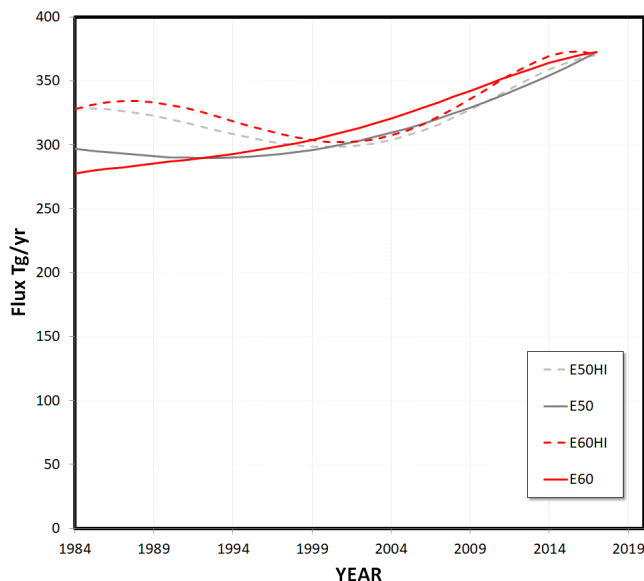
Fig. S5. Plot of the anthropogenic component of the flux (Tg/yr) for the four scenarios explored in the model. E50 and E60 broadly reproduce smoothed (5th order) fits to fluxes in EDGAR 6.0 and 5.0 (1). The lines labeled E60HI and E50HI use natural gas flux that broadly reproduces a 5th order fit to the natural gas flux of Höglund-Isaksson (2), but with other fluxes similar to those in the EDGAR.
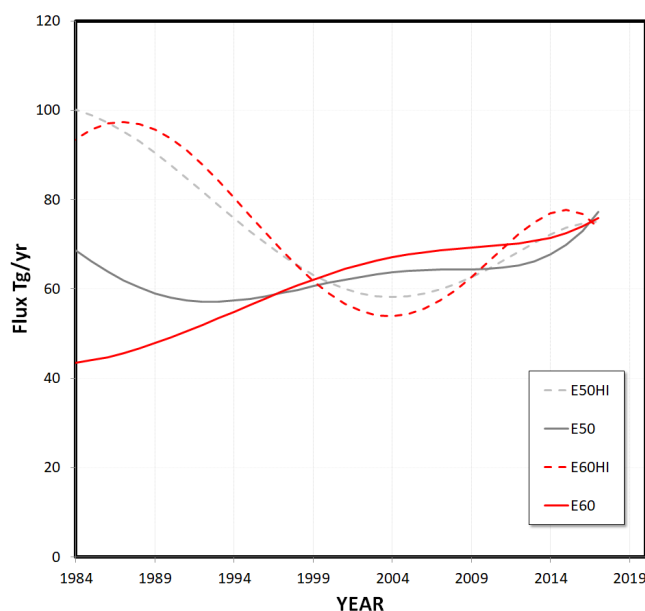
Fig. S6. Flux of methane from natural gas for the four different scenarios explored in the model. E50 and E60 broadly reproduce smoothed (5th order) fits to fluxes in EDGAR 6.0 and 5.0 (1), and HI broadly reproduces a 5th order fit to the Natural Gas flux of Höglund-Isaksson (2), but with other fluxes similar to those in the EDGAR.
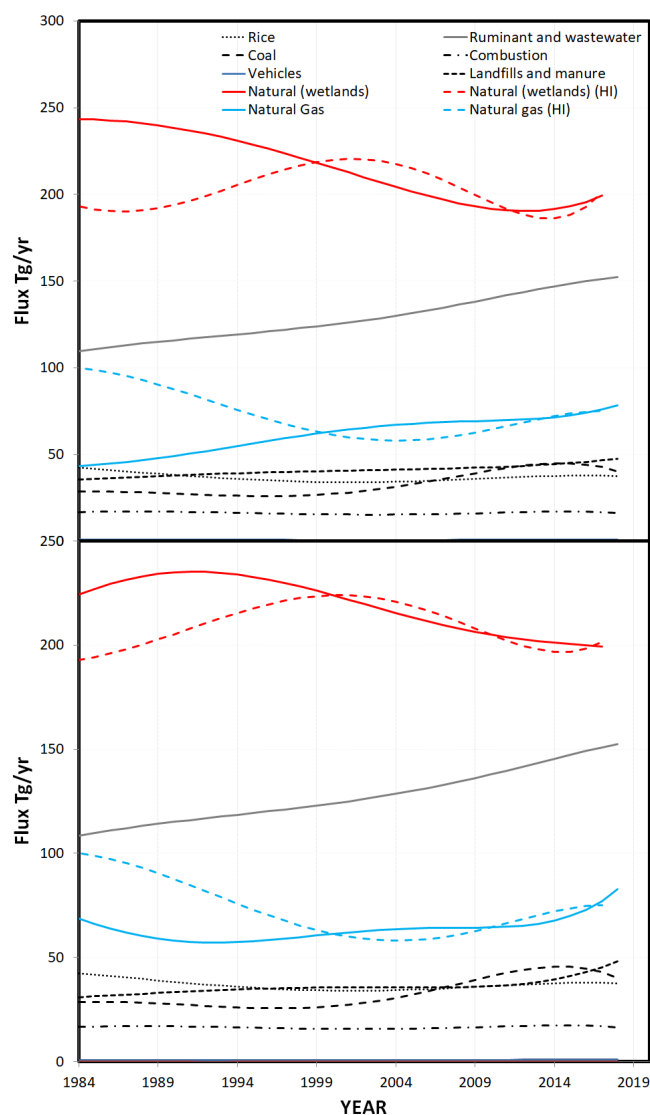
Fig. S7. Plot of the flux of methane (Tg/yr) for natural sources (treated as wetlands) and component anthropogenic sources for the four model scenarios (defined as in prior figures and captions). The flux from natural sources for our different scenarios was determined by subtracting total anthropogenic flux from the total flux. Where there are no (HI) curves, the flux profiles are the same. Panel A. is E50 and E50HI fluxes. Panel B. is E60 and E60HI fluxes.
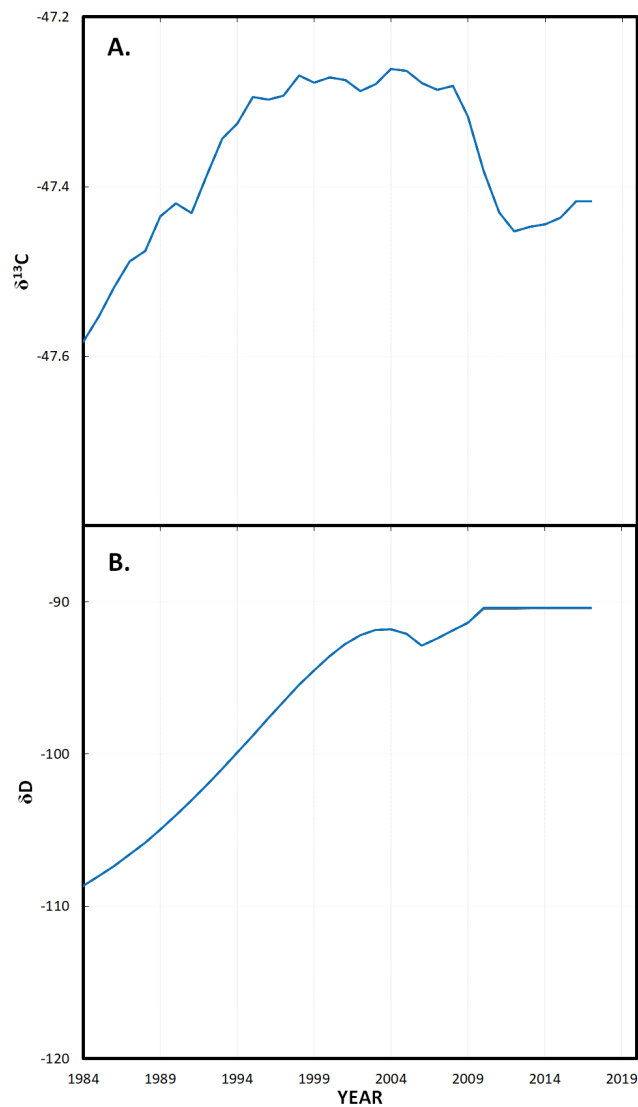
Fig. S8. A. Plot of $\delta^{13}C$ for methane in air used as a constraint for the model. The evolution broadly follows that presented by Turner et al., (*5*) and is derived by tracing his curve. **B.** Plot of δD for methane in air used as a constraint for the model. The evolution broadly follows that presented by Rice et al., (*6*) until 2010 (derived by tracing his curve).
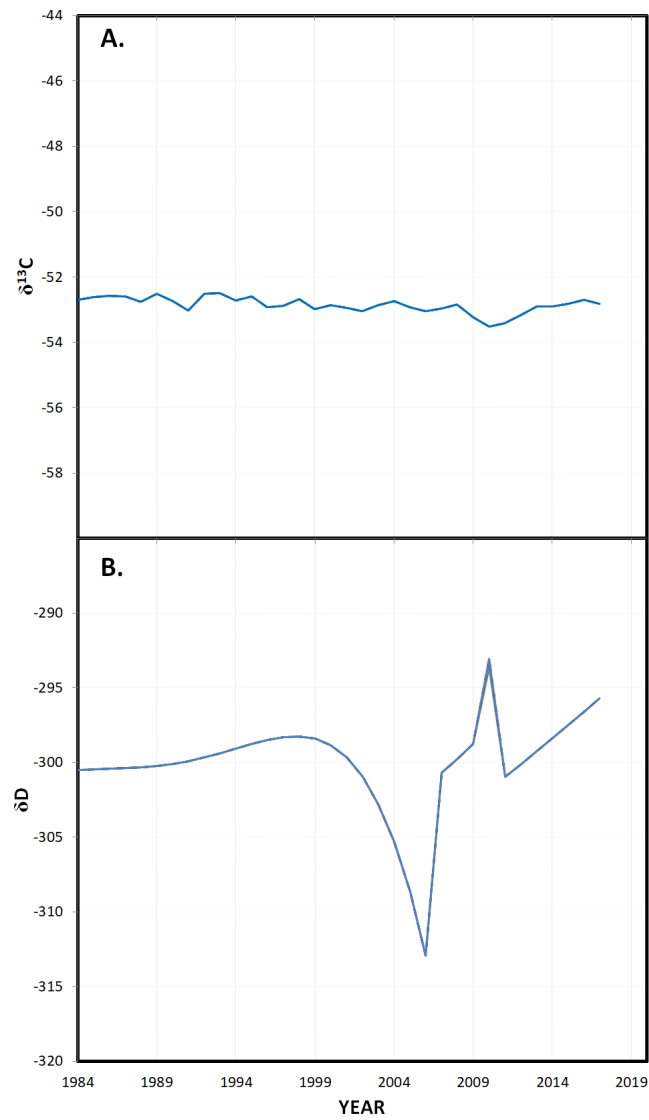
Fig. S9. A. Plot of δ¹³C for source CH₄ to air derived using equation 5. **B.** Plot of δD for source CH₄ (methane flux) to air derived using equation 5. Shape of each is influenced by changes in profiles of δ¹³C and δD of methane in air (**Figure S8.**)
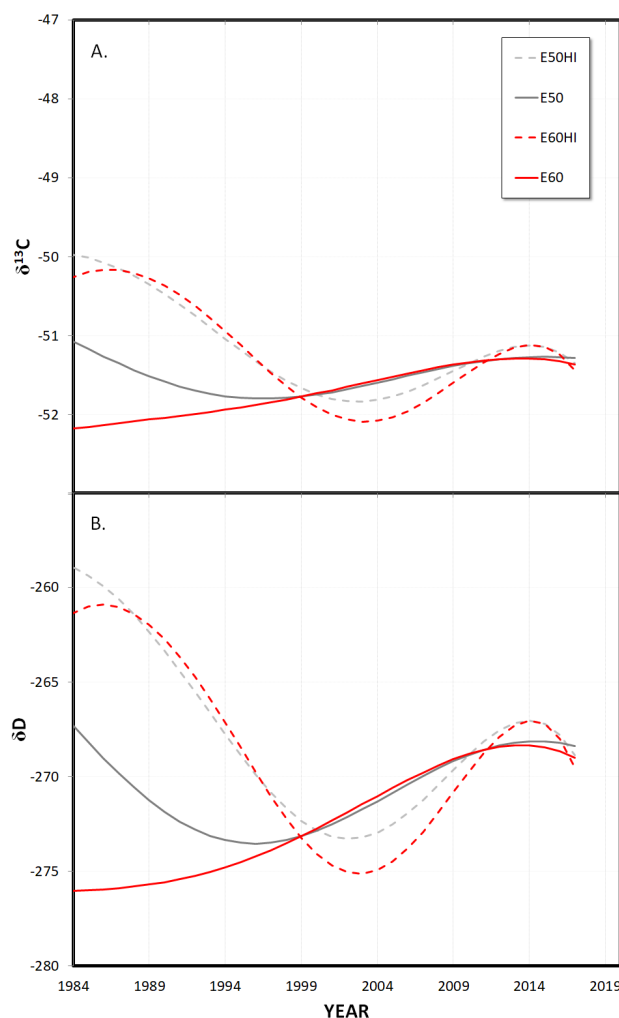
Fig. S10 Isotope profiles for anthropogenic part of total flux of model scenarios **A.** Plot of carbon isotope compositions used in model for anthropogenic endmember. **B.** Plot of deuterium/hydrogen isotope compositions used in models for anthropogenic endmember. These values are calculated using source apportionment in the four scenarios which are smoothed (5th order functions) that broadly follow the flux apportionment given in EDGAR 6.0 (E60), EDGAR 5.0 (E50), EDGAR 6.0 with natural gas fluxes of (2) (E60HI) and EDGAR 5.0 with natural gas fluxes of (37) (E50HI).
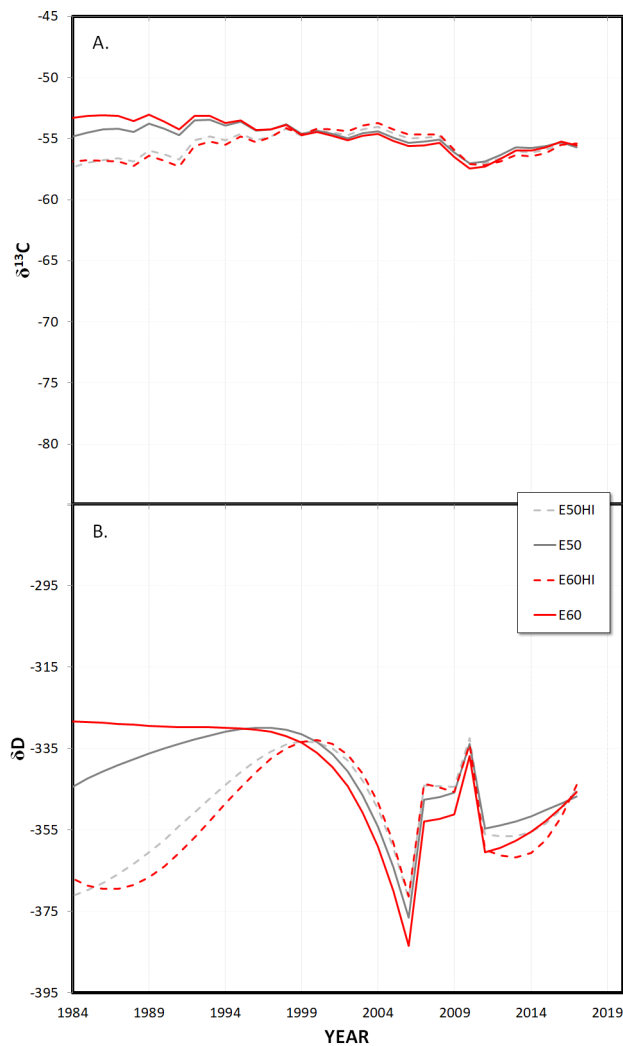
Figure S11. Plot of δ^{13}C (**Panel A.**) and δD (**Panel B.**) for the natural (wetland) methane part of the flux generated by the model. The isotopic compositions are those required to make up the isotopic balance needed to reproduce the isotopic compositions of the total flux (**Figure S.4**) after the isotopic composition of the anthropogenic part (**Figures S7**) of the flux is accounted for.
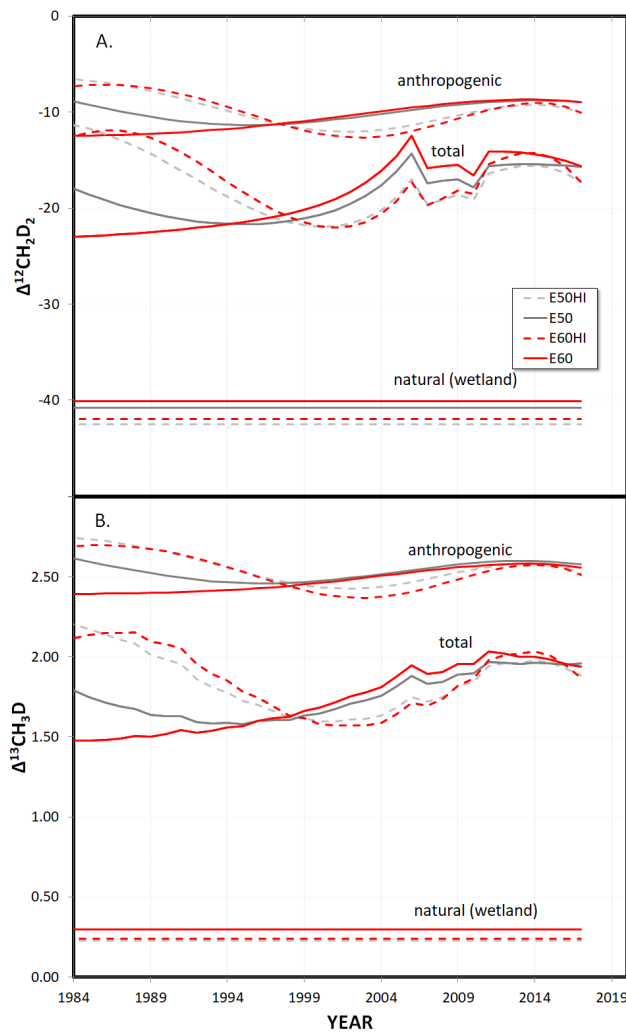
Fig. S12. Plot of $\Delta^{12}CH_2D_2$ (**Panel. A**) and $\Delta^{13}CH_3D$ (**Panel. B**) for methane of sources (fluxes) to air for the four model scenarios from the anthropogenic part, the natural (wetland) part, and of the total. The total for $\Delta^{12}CH_2D_2$ shows small breaks in slope which reflect the fit to δD because δD is part of the calculation of $\Delta^{12}CH_2D_2$. Likewise, similar variations and a less smooth relationship shows up for total $\Delta^{13}CH_3D$ because of the added effect of variability in the fit for $\delta^{13}C$.
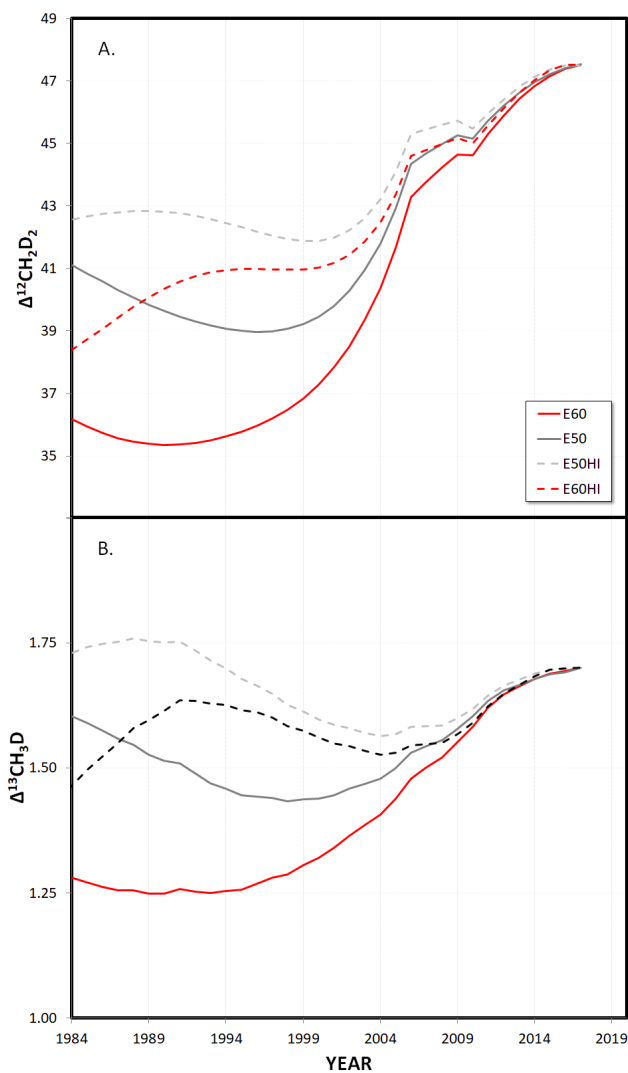
Fig. S13. Plot of $\Delta^{12}CH_2D_2$ (**Panel. A**) and $\Delta^{13}CH_3D$ (**Panel. B**) for methane of .air for the four model scenarios.
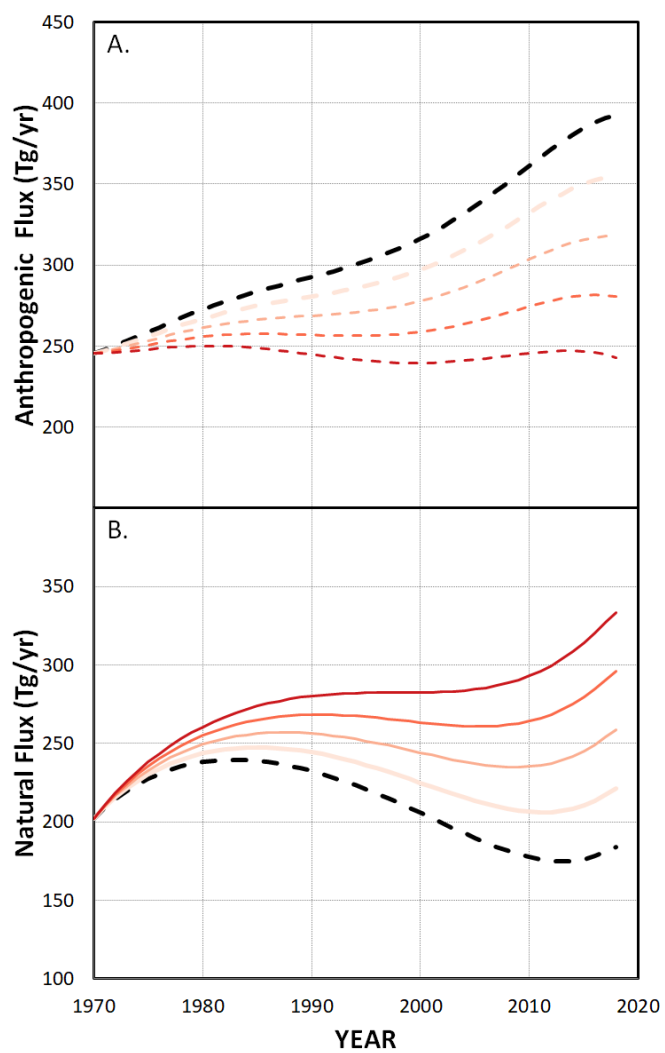
Figure S14. Plot of fluxes used in the second set of models. Total source is kept constant. **A.** Fluxes from anthropogenic components. **B.** fluxes from the natural (wetland) component.
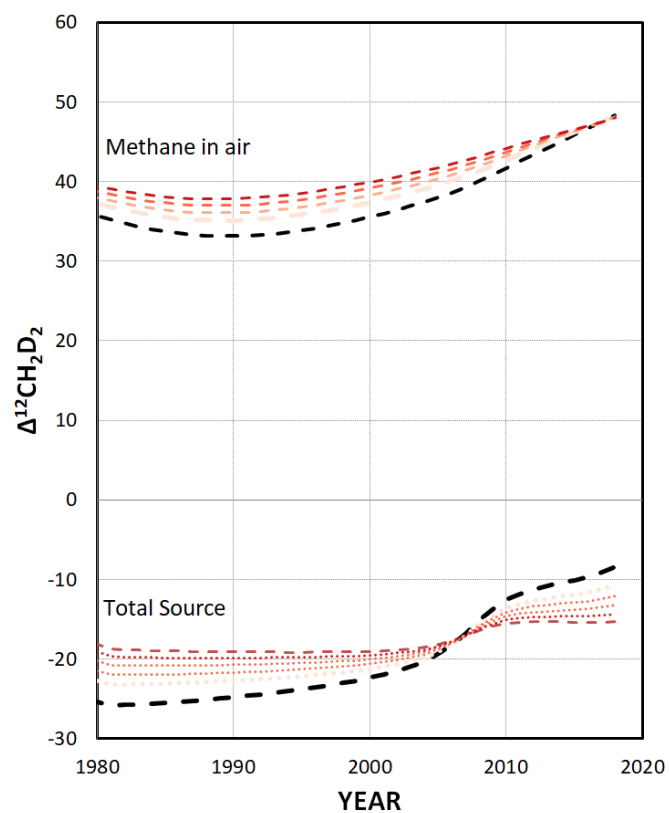
Fig. S15. Plot of $\Delta^{12}CH_2D_2$ for model scenarios ranging from rising anthropogenic CH_4 flux and stable wetlands CH_4 flux (black dashed) to flat anthropogenic methane and rising wetland CH_4 flux (red curves).
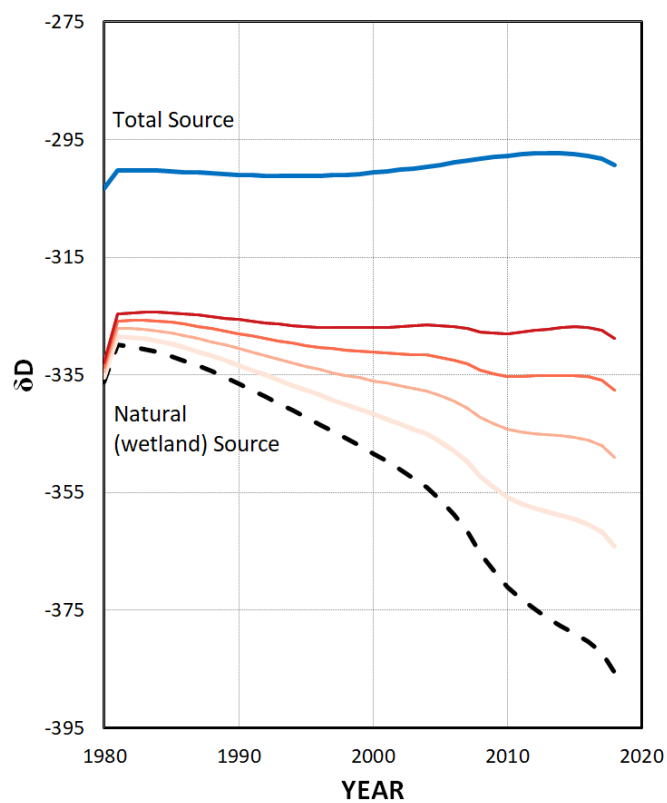
Fig. S16. Plot of δD for total source (blue line) and for the natural (wetland) portion of the total source (black and red lines as defined in previous plots). The dashed black line is for a rising anthropogenic flux and stable natural flux and the red lines progress to a rising natural (wetland) flux.
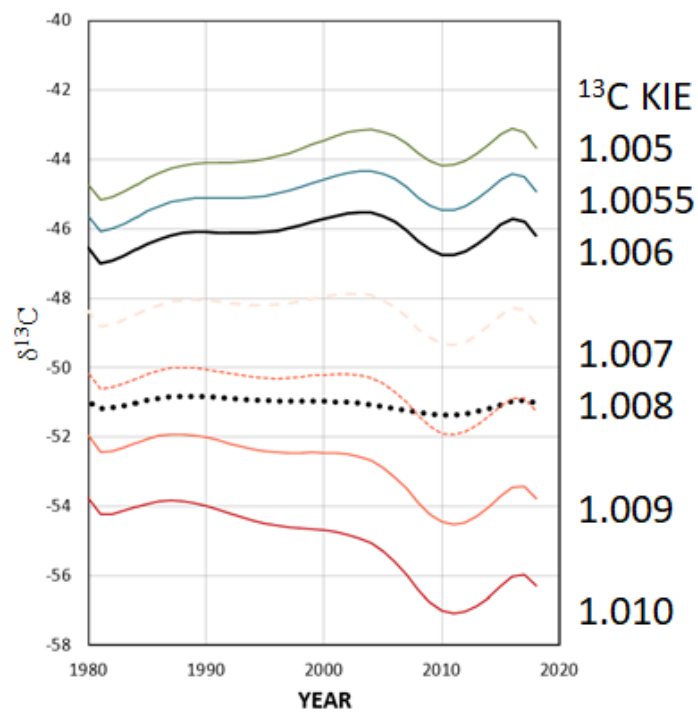
Fig. S17. Plot of model result calculated using different values for the $^{13}CH_4$ sink reaction. A value of 1.006 used in this study based on ab initio methods yields values that are less negative for the natural (wetland) part of the source flux than the total flux. A KIE value closer to 1.010 would reverse this.
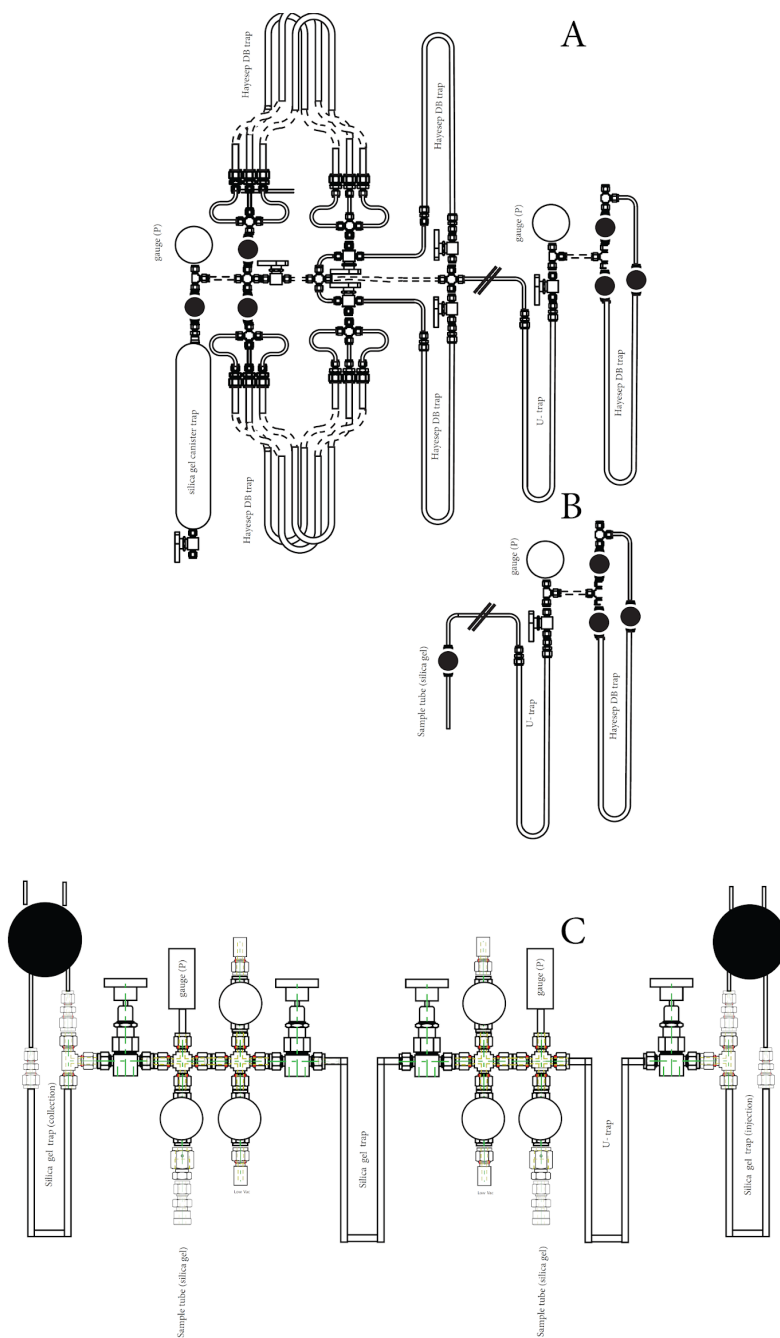
Fig. S18 Schematic of air preconcentration manifold and purification manifold. Pumps used during preconcentration are Gast two stage diaphragm pumps, followed by a rotary vane pump for final pumping. Pumps used on the purification manifold are a rotary vane pump for rough vacuum and a small turbo pump repurposed from a decommissioned mass spectrometer. The GC is an SRI with TCD.
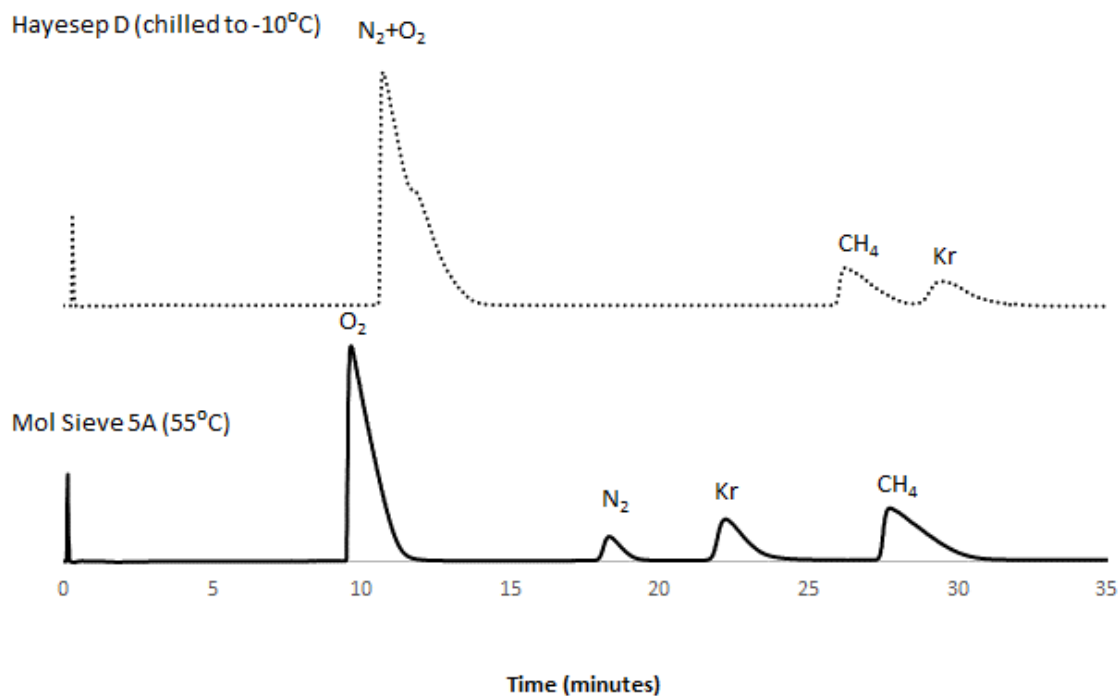
Fig. S19 Sample chromatograms illustrating separation of pre-concentrated gases (N2, O2, Kr, CH4) using HayeSep D column and Molecular Sieve Column. The HayeSep D column did not separate the CH_4 and Kr when used at temperatures >20°C. The column was cooled by modifying the inlet fan to the oven with a U shape in ducting that was filled with a small amount of liquid nitrogen (a kluge for testing and separating/confirming the second peak as Kr). The lower trace is for a molecular sieve 5A column at 55°C and the separation of all permanent gases is better and more predictable.

Isotopologue data

Table S1. Measured isotopologue data of samples

Sample type	Sample number	$\delta^{13}CH_4$ (‰)	2σ	$\delta^{12}CH_3D$ (‰)	2σ	$\delta^{13}CH_3D$ (‰)	2σ	$\delta^{12}CH_2D_2$ (‰)	2σ	$\Delta^{13}CH_3D$ (‰)	2σ
Air (Airgas tank)	210419	-47.84	0.03	-111.64	0.13	-153.27	0.96	-168.51	1.73	1.03	1.15
Air (Airgas tank)	210421	-47.93	0.03	-112.72	0.11	-154.61	0.84	-174.88	1.60	0.76	1.00
Air (local mix - Barn)	210423	-64.16	0.02	-321.79	0.04	-364.96	0.50	-551.34	0.74	0.55	0.79
Air (local mix - Barn)	210803b2	-53.94	0.07	-210.10	0.40	-250.72	1.05	-354.14	3.33	2.67	1.50
Air (local mix - Barn)	210803b3	-57.30	0.02	-236.01	0.08	-278.62	0.47	-404.37	1.47	1.62	0.66
Air (local mix - Barn)	210803B1	-58.24	0.02	-242.67	0.10	-285.14	0.49	-416.03	1.69	2.31	0.69
Air (local mix - campus Farm)	210720S	-47.61	0.04	-112.11	0.34	-153.29	0.74	-174.32	2.54	1.29	0.95
Air (local mix - campus Farm)	210720B	-45.84	0.05	-93.60	0.41	-134.70	0.80	-140.17	2.33	0.52	1.03
Air (local mix - campus Farm)	210803S10	-46.83	0.06	-108.81	0.22	-148.96	0.86	-169.67	2.43	1.87	1.05
Air (local mix - campus Farm)	210803-S4	-47.68	0.02	-133.02	0.22	-173.50	0.55	-237.46	2.42	1.03	0.72
Air (local mix - campus Farm)	210904s4	-47.35	0.02	-107.32	0.18	-148.61	0.45	-166.12	2.02	1.16	0.56
Air (local mix - wetland)	210429	-49.17	0.03	-120.07	0.13	-161.89	0.98	-186.18	1.74	1.74	1.18
Air (local mix -wetland)	210429	-52.41	0.02	-223.82	0.07	-263.07	0.52	-381.46	1.22	1.95	0.71
Air (local mix -wetland)	210418	-49.31	0.02	-135.94	0.06	-177.48	0.67	-220.24	1.13	1.31	0.82
Air (urban - chemistry bldg.)	210901	-47.13	0.03	-92.21	0.15	-133.59	0.71	-138.87	1.84	1.63	0.84

Air (urban - chemistry bldg.)	210329	-47.44	0.03	-91.41	0.09	-133.24	0.72	-134.41	1.49	1.48	0.83
Air (urban - chemistry bldg.)	210408	-47.39	0.04	-89.33	0.12	-131.32	0.92	-132.59	1.66	1.34	1.07
Air (urban - chemistry bldg.)	21503	-47.28	0.03	-91.73	0.10	-132.05	0.67	-138.72	1.45	3.03	0.79
Air (urban - chemistry bldg.)	21504	-47.58	0.03	-89.01	0.17	-130.88	0.84	-132.42	2.10	1.70	0.98
Air (urban - chemistry bldg.)	210506	-47.93	0.02	-90.37	0.12	-132.25	0.64	-132.94	1.72	1.99	0.75
Air (urban - chemistry bldg.)	210511	-47.65	0.02	-91.46	0.09	-133.12	0.52	-133.89	1.61	1.88	0.61
Air (urban - chemistry bldg.)	210514	-48.06	0.02	-90.98	0.10	-132.54	0.65	-134.32	1.60	2.46	0.76
Air (urban - shoppers parking lot)	210805	-46.56	0.05	-96.32	0.31	-136.81	0.65	-144.31	2.57	1.85	0.83
Burning (charcoal)	210515b	-28.80	0.01	-256.12	0.05	-275.60	0.26	-456.68	0.86	2.69	0.37
Burning (Oak)	210515A/23	-26.54	0.02	-241.04	0.04	-259.97	0.26	-432.32	0.83	1.63	0.36
Chamber (wetland - rice paddy)	210819	-62.28	0.01	-334.07	0.08	-376.67	0.43	-575.69	1.55	-1.80	0.69
Chamber (wetland)	210420d/e	-53.56	0.05	-306.37	0.15	-343.47	0.44	-533.80	1.24	0.07	0.71
Chamber (wetland)	210420BC	-54.91	0.02	-318.82	0.05	-355.53	0.29	-554.02	0.77	1.08	0.46
Chamber (wetland)	210420H	-52.02	0.02	-320.85	0.05	-356.09	0.46	-557.21	0.84	0.15	0.72
Chamber (wetland)	210409	-47.23	0.02	-332.88	0.05	-365.57	0.46	-580.40	0.71	-1.86	0.72
Incubation	210429i	-59.43	0.07	-309.97	0.18	-351.34	0.96	-541.34	1.44	-0.57	1.51
Incubation	210430i	-60.08	0.02	-327.32	0.06	-368.44	0.62	-569.48	0.83	-1.11	0.98
Incubation	210524i	-70.48	0.04	-340.30	0.24	-386.29	0.64	-584.16	1.69	0.84	1.10

Natural gas	210506n	-35.19	0.02	-163.92	0.07	-190.91	0.38	-293.56	0.99	3.01	0.48
Natural gas	211218n	-34.33	0.03	-157.34	0.08	-185.79	0.29	-284.09	0.92	0.59	0.37
Natural gas	211221n	-22.79	0.03	-156.66	0.13	-174.59	0.47	-283.70	1.48	1.57	0.59

Table S2 Thermal Equilibration data

Sample number	$\delta^{13}CH_4$ (‰)	2σ	$\delta^{13}CH_3D$ (‰)	2σ	$\delta^{12}CH_3D$ (‰)	2σ	$\delta^{12}CH_2D_2$ (‰)	2σ	$\Delta^{13}CH_3D$ (‰)	2σ	$\Delta^{12}CH_2D_2$ (‰)	2σ
Starting Methane	-37.00		-178.24		-149.20		-270.66		2.98		7.58	
230424 150	-34.29	0.01	-172.86	0.26	-146.14	0.05	-265.35	1.25	3.10	0.32	7.65	1.71
230424 32	-37.00	0.02	-175.92	0.31	-148.97	0.05	-262.54	1.09	5.54	0.38	18.23	1.51
230424-15	-36.98	0.02	-175.13	0.20	-148.73	0.05	-260.08	0.92	6.20	0.26	21.06	1.28

Table S3. Isotopologue values comparison for samples analyzed by UCLA (25)) and MIT (27), and UMD.

	Sample	$\delta^{13}CH_4$ (‰)	2σ	$\delta^{12}CH_3D$ (‰)	2σ	$\Delta^{13}CH_3D$ (‰)	2σ	$\Delta^{12}CH_2D_2$ (‰)	2σ
MIT	AL1	-34.50	0.02	-147.70	0.06	2.33	0.05	4.40	0.50
	AL1-CD	-82.44	0.72	-158.00	0.18	15.79	0.45	5.50	1.90
	AL1-D3	-35.24	0.06	239.81	0.15	1.49	0.14	26.40	0.60
UCLA	AL1	-34.65	0.01	-147.88	0.09	2.41	0.26	5.62	0.87
	AL1-CD	-82.01	0.03	-159.72	0.03	16.13	0.30		
	AL1-D3	-34.76	0.00	242.55	0.01	1.55	0.12		
UMD	AL1‡	-34.5	0.01	-147.7	0.14	2.62	0.41	5.68	1.56
	AL1-CD	-82.14	0.01	-159.30	0.06	16.07	0.21	10.98	1.18
	AL1-D3	-34.77	0.01	242.13	0.10	1.68	0.22	26.79	1.23

[‡] Assigned based on MIT Value and three thermal equilibration experiments because used as basis for standardization

Table S4. Isotopologue values comparison for three different composite samples including a reference gas, wetland sample and air sample analyzed by Caltech and UMD.

	Sample	$\delta^{13}CH_4$ (‰)	2σ	$\delta^{12}CH_3D$ (‰)	2σ	$\Delta^{13}CH_3D$ (‰)	2σ	$\Delta^{12}CH_2D_2$ (‰)	2σ
Caltech	220202a	-37.01	0.02	-145.04	0.32	3.07	0.96	9.1	3.20
	220122a	-49.91	0.04	-325.52	0.34	0.77	1.22	-46.4	4.60
	220121a	-46.67	0.02	-91.03	0.54	0.01	1.04	53	4.00
UMD	220202a[§]	-36.95		-149.0		2.98		7.58	
	220122a	-49.30	0.01	-333.30	0.06	-1.85	0.27	-50.74	1.78
		-49.28	0.01	-332.80	0.02	-2.69	0.75	-50.66	3.61
	220121a	-46.21	0.02	-93.92	0.11	2.17	0.57	45.01	2.04
		-46.19	0.03	-93.85	0.14	0.56	0.37	47.93	2.40
		-45.90	0.02	-94.08	0.12	1.23	0.71	47.56	2.26

[§] Assigned based on MIT Value and three thermal equilibration experiments because used as basis for standardization

Table 5 Conversions to transform EDGAR data into isotopic compositions for models.

This study	ipcc_code_2006_ for_standard_re port	ipcc_code_2006_for_standard_report_name
Combustion	1.A.1.a	Main Activity Electricity and Heat Production
Combustion	1.A.1.a	Main Activity Electricity and Heat Production
Combustion	1.A.1.bc	Petroleum Refining - Manufacture of Solid Fuels and Other Energy Industries
Combustion	1.A.1.bc	Petroleum Refining - Manufacture of Solid Fuels and Other Energy Industries
Combustion	1.A.2	Manufacturing Industries and Construction
Combustion	1.A.2	Manufacturing Industries and Construction
Combustion	1.A.3.a	Civil Aviation
Vehicles	1.A.3.b_noRES	Road Transportation no resuspension
Vehicles	1.A.3.b_noRES	Road Transportation no resuspension
Vehicles	1.A.3.c	Railways
Vehicles	1.A.3.c	Railways
Vehicles	1.A.3.d	Water-borne Navigation
Vehicles	1.A.3.d	Water-borne Navigation
Vehicles	1.A.3.e	Other Transportation
Vehicles	1.A.3.e	Other Transportation
Combustion	1.A.4	Other Sectors
Combustion	1.A.4	Other Sectors
Combustion	1.A.5	Non-Specified
Combustion	1.A.5	Non-Specified
COAL Fugitive	1.B.1	Solid Fuels
COAL Fugitive	1.B.1	Solid Fuels

Natural gas Fugitive	1.B.2	Oil and Natural Gas
Natural gas Fugitive	1.B.2	Oil and Natural Gas
production and fugitive	2.B	Chemical Industry
Hight-T	2.C	Metal Industry
Rumen	3.A.1	Enteric Fermentation
Manure	3.A.2	Manure Management
Biomass Burning	3.C.1	Emissions from biomass burning
Rice	3.C.7	Rice cultivations
biogenic Landfill	4.A	Solid Waste Disposal
biogenic Landfill	4.B	Biological Treatment of Solid Waste
Burning	4.C	Incineration and Open Burning of Waste
Burning	4.C	Incineration and Open Burning of Waste
Wastewater treatment	4.D	Wastewater Treatment and Discharge
Other	5.B	Other

Table S6 KIE used in model simulations

	KIE	k'/k
$^{12}CH_4$	1.0000	1.00000
$^{13}CH_4$	1.0060	0.99400
$^{12}CH_3D$	1.3213	0.75683
$^{13}CH_3D$	1.3135	0.76135
$^{12}CH_2D_2$	1.8613	0.53726

Table S7. Isotopic compositions of Category

	δ¹³C	δ¹³CH₃D	δD	δ¹²CH₂D2	Δ¹³CH₃D	Δ¹²CH₂D2
			$E60$			
Rice	-63.0	-362.7	-320.0	-556.2	0.30	-40.3
Ruminants and wastewater	-60.5	-370.3	-330.0	-569.2	0.30	-40.3
Natural gas	-39.6	-210.1	-180.0	-322.5	3.00	7.6
Coal	-37.0	-169.3	-140.0	-254.8	3.00	7.6
Combustion	-24.6	-241.9	-225.0	-409.0	2.80	-16.0
Vehicles	-24.6	-242.6	-225.0	-396.4	2.00	5.0
High T	-24.6	-243.7	-225.0	-398.8	0.50	1.0
Landfills and manure	-55.0	-347.8	-310.0	-543.1	0.30	-40.3
Biomass burning	-41.0	-254.7	-225.0	-409.0	2.80	-16.0
			$E60HI$			
Rice	-63.0	-362.7	-320.0	-557.0	0.24	-41.9
Ruminants and wastewater	-60.5	-370.4	-330.0	-569.9	0.24	-41.9
Natural gas	-39.6	-210.1	-180.0	-322.5	3.00	7.6
Coal	-37.0	-169.3	-140.0	-254.8	3.00	7.6
Combustion	-24.6	-241.9	-225.0	-409.0	2.80	-16.0
Vehicles	-24.6	-242.6	-225.0	-396.4	2.00	5.0
High T	-24.6	-243.7	-225.0	-398.8	0.50	1.0
Landfills and manure	-55.0	-347.8	-310.0	-543.9	0.24	-41.9
Biomass burning	-41.0	-254.7	-225.0	-409.0	2.80	-16.0
			$E50$			
Rice	-63.0	-362.7	-320.0	-556.5	0.30	-40.8
Ruminants and wastewater	-60.5	-370.3	-330.0	-569.4	0.30	-40.8
Natural gas	-39.6	-210.1	-180.0	-322.5	3.00	7.6
Coal	-37.0	-169.3	-140.0	-254.8	3.00	7.6

Combustion	-24.6	-241.9	-225.0	-409.0	2.80	-16.0
Vehicles	-24.6	-242.6	-225.0	-396.4	2.00	5.0
High T	-24.6	-243.7	-225.0	-398.8	0.50	1.0
Landfills and manure	-55.0	-347.8	-310.0	-543.3	0.30	-40.8
Biomass burning	-41.0	-254.7	-225.0	-409.0	2.80	-16.0

<div align="center">E50HI</div>

Rice	-63.0	-362.7	-320.0	-557.2	0.23	-42.5
Ruminants and wastewater	-60.5	-370.4	-330.0	-570.2	0.23	-42.5
Natural gas	-39.6	-210.1	-180.0	-322.5	3.00	7.6
Coal	-37.0	-169.3	-140.0	-254.8	3.00	7.6
Combustion	-24.6	-241.9	-225.0	-409.0	2.80	-16.0
Vehicles	-24.6	-242.6	-225.0	-396.4	2.00	5.0
High T	-24.6	-243.7	-225.0	-398.8	0.50	1.0
Landfills and manure	-55.0	-347.8	-310.0	-544.1	0.23	-42.5
Biomass burning	-41.0	-254.7	-225.0	-409.0	2.80	-16.0

Grey fields are determined by model fit for wetlands and assigned to all microbial sources.

Table S8. Derived clumped isotopologue compositions for different model scenarios.

	$\Delta^{13}CH_3D$	$\Delta^{12}CH_2D2$
E60	0.30	-40.13
E60HI	0.24	-41.96
E50	0.30	-40.77
E50HI	0.23	-42.49

Table S9. Tests of recovery of 40 micromole (1cc) methane from 200 L nitrogen

Sample number	$\delta^{13}CH_4$ (‰)	2σ	$\delta^{12}CH_3D$ (‰)	2σ	$\Delta^{13}CH_3D$ (‰)	2σ	$\Delta^{12}CH_2D_2$ (‰)	2σ
Starting	-37.00		-149.20		2.98		7.58	
230330	-36.84	0.01	-148.54	0.16	2.76	0.35	8.36	2.66
230221	-36.82	0.02	-148.44	0.22	2.72	0.45	9.24	3.18